Comptes Rendus
Géoscience — Sciences de la Planète
Supplementary material to the article available at:
https://doi.org/10.5802/crgeos.233

Supplementary material: Hard rock aquifer architecture and water circulation levels in the Strengbach critical zone observatory (France)

François Chabaux[*, a], Philippe Négrel[*, b], Frederick Gal[*, b], Daniel Viville[a], Coralie Ranchoux[a], Jérome Van der Woerd[a], Frederick Delay[a], Julien Ackerer[a], Luc Aquilina[c], Marc Diraison[a], Frédéric Masson[a], Anne-Sophie Mériaux[a], Thierry Labasque[c], Yann Lucas[a], Philippe Adrien Pezard[d], Thierry Reuschlé[a], Anne-Désirée Schmitt[a], Peter Stille[a], Robert Wyns[b], Catherine Lerouge[*, b] and Chrystel Dezayes[*, b]

[a] Institut Terre et Environnement de Strasbourg, Université de Strasbourg, CNRS, ENGEES, 67000 Strasbourg, France

[b] BRGM, 45060 Orléans, France

[c] Géosciences Rennes, Université Rennes, CNRS, 35000 Rennes, France

[d] Géosciences Montpellier, CNRS, Université de Montpellier, Place Eugène Bataillon, 34000 Montpellier, France

E-mails: fchabaux@unistra.fr (F. Chabaux), p.negrel@brgm.fr (P. Négrel), f.gal@brgm.fr (F. Gal), c.lerouge@brgm.fr (C. Lerouge), c.dezayes@brgm.fr (C. Dezayes)

Not yet published

Supplementary Table S1. Fracture orientations from oriented borehole wall images

Supplementary Table S2. Porosity and permeability data from core

* Corresponding authors.

1. Longitudinal schematic section of the wells showing the main equipment on each of them

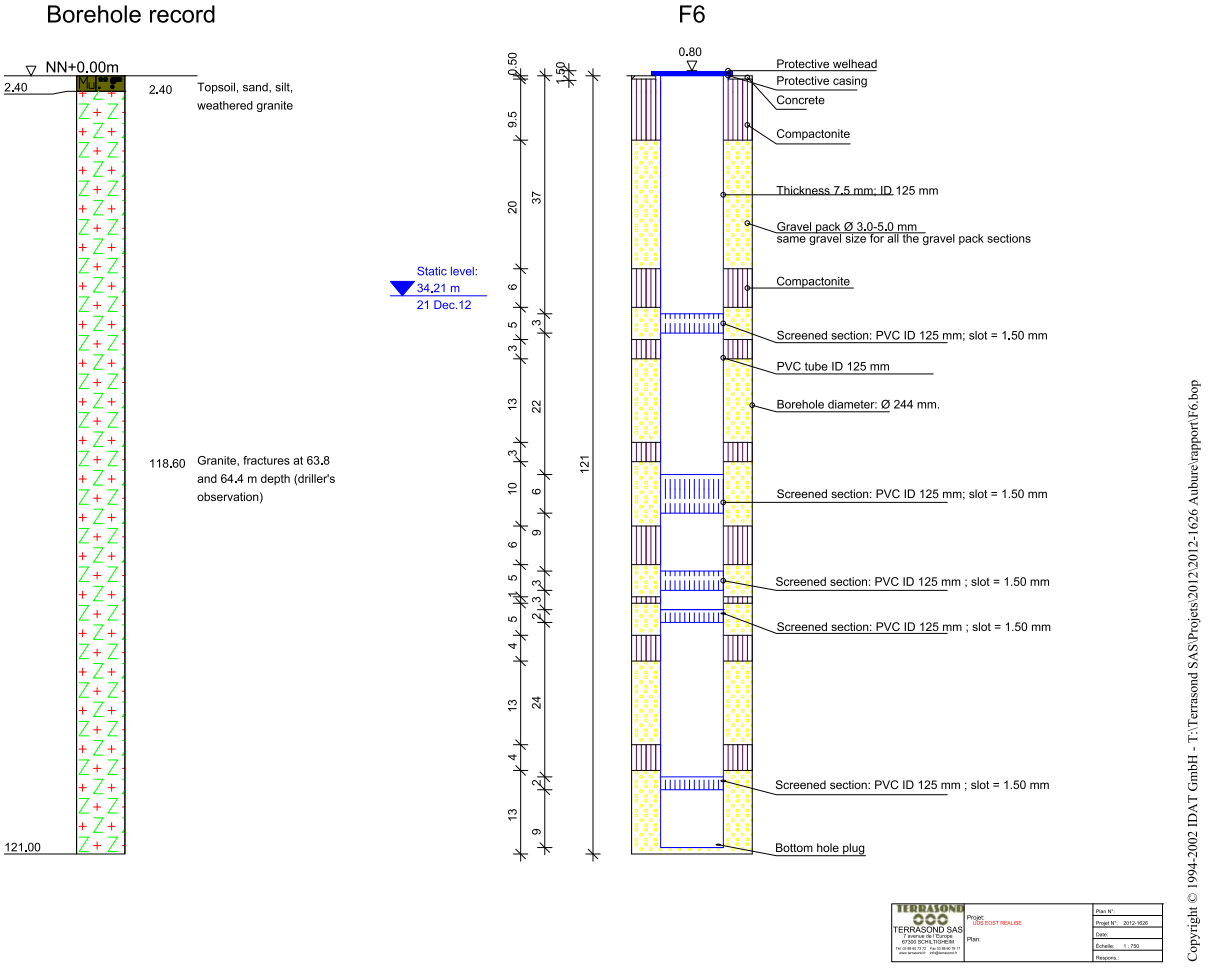

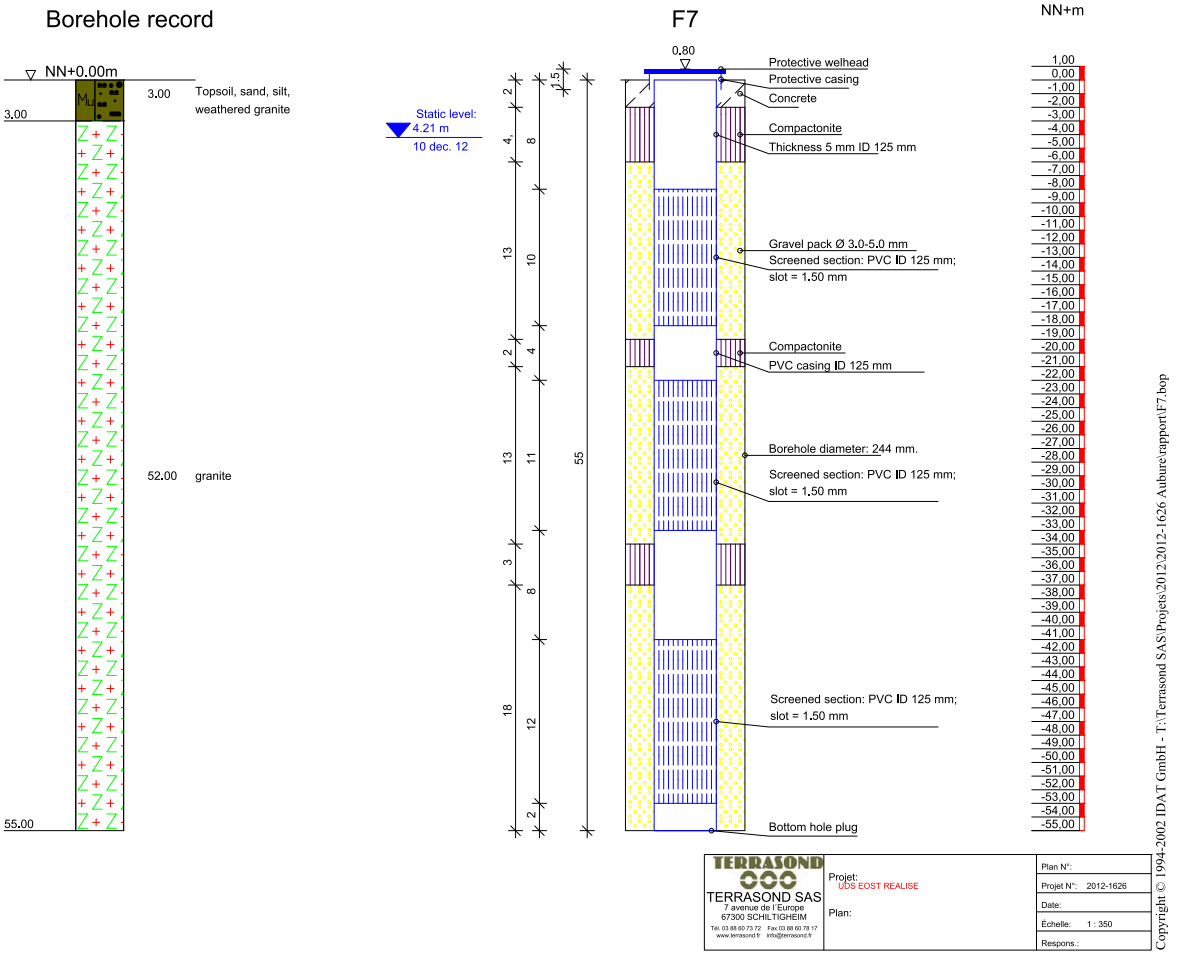

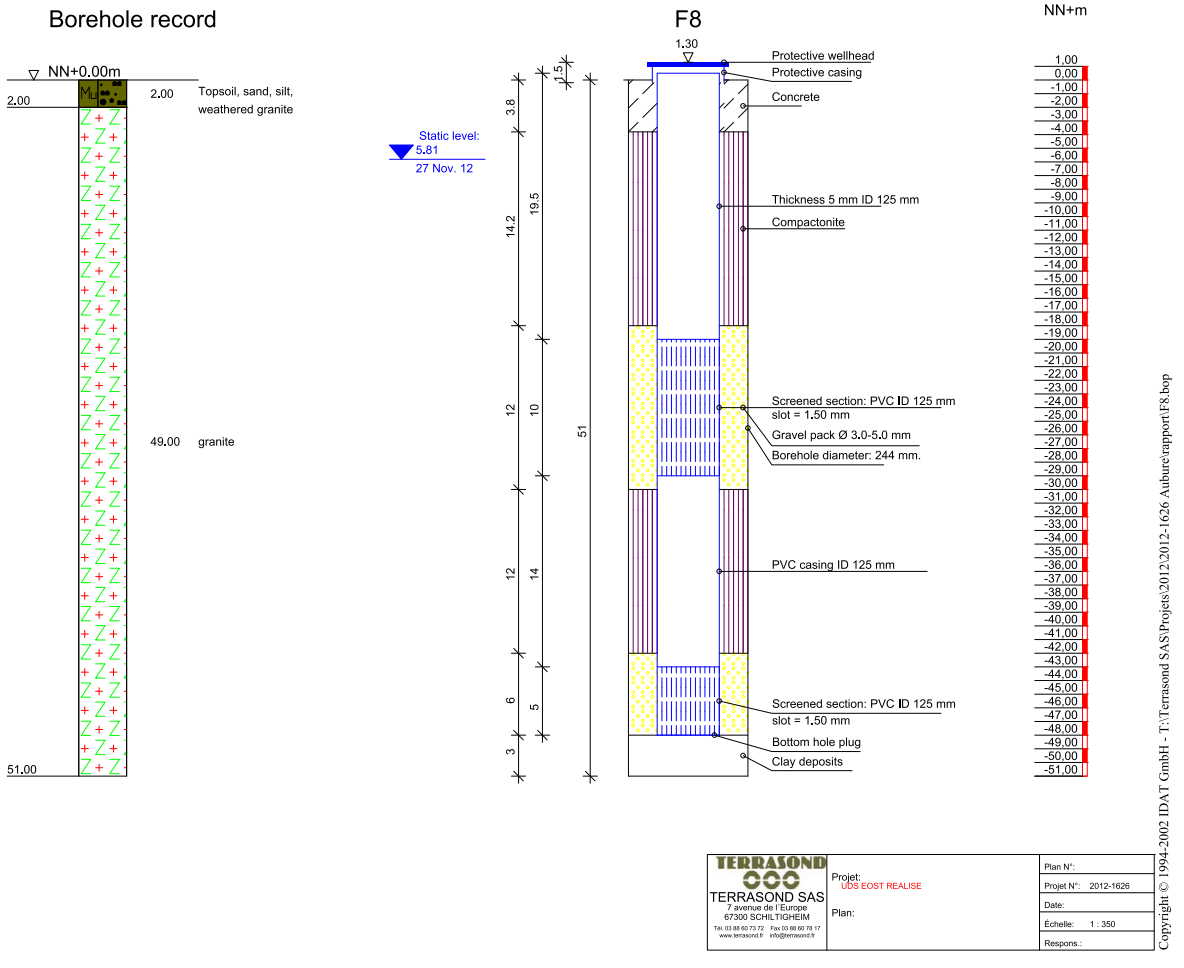

TERRASOND
TERRASOND SAS
7 avenue de l'Europe
67300 SCHILTIGHEIM
Tél. 03 88 60 73 72 Fax 03 88 60 78 17
www.terrasond.fr info@terrasond.fr

Projet: UDS EOST REALISE
Plan:

Plan N°:
Projet N°: 2012-1626
Date:
Échelle: 1 : 350
Respons.:

Stölben GmbH
Barlstraße 42
56856 Zell/Mosel
Tel: +49 6542 9366-0
e-mail: info@stoelben-gmbh.de

Projet N° 25058_CNRS

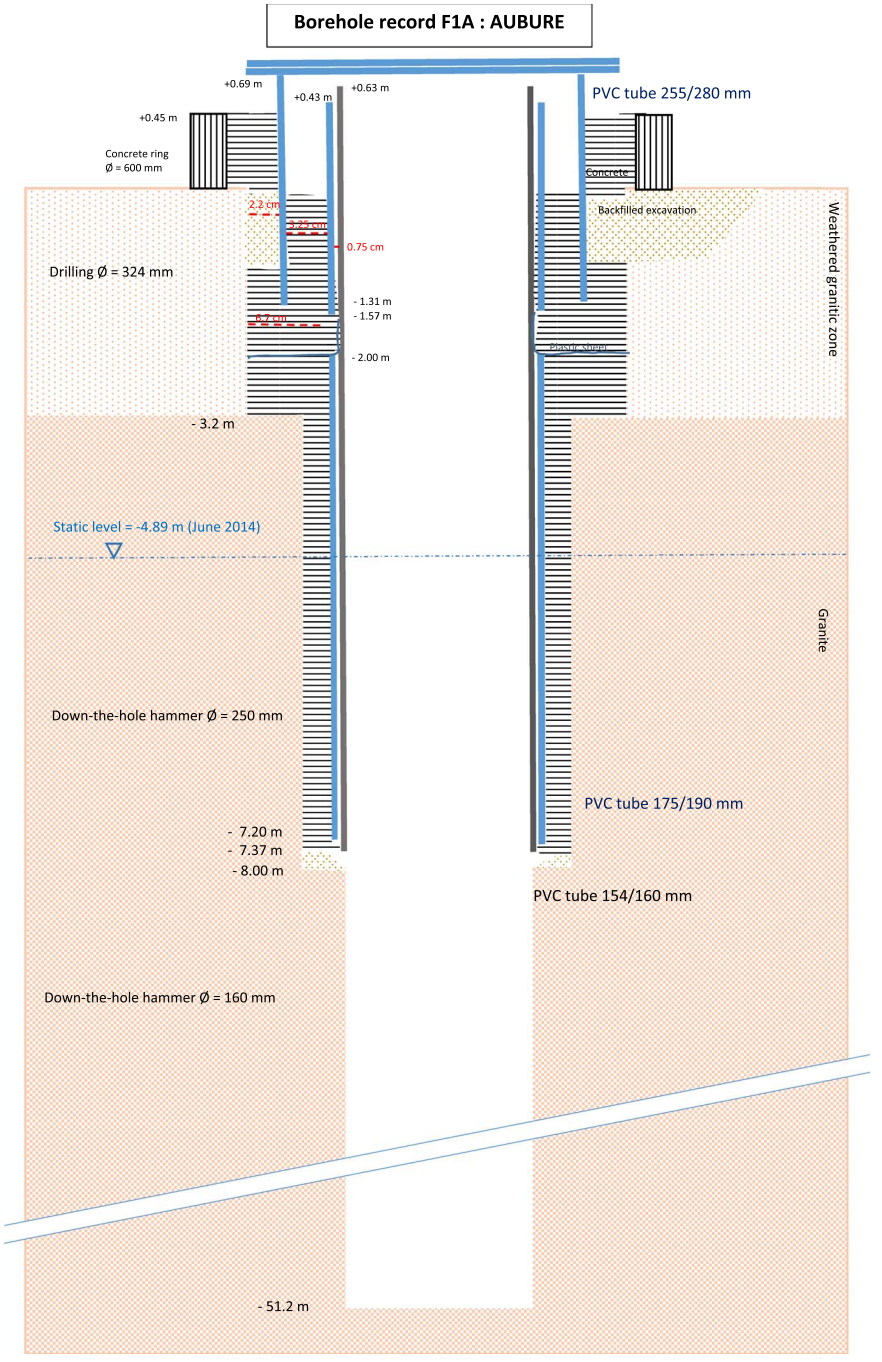

Stölben GmbH
Barlstraße 42
56856 Zell/Mosel
Tel: +49 6542 9366-0
e-mail: info@stoelben-gmbh.de

Projet N° 25058_CNRS

Borehole record F1B : AUBURE

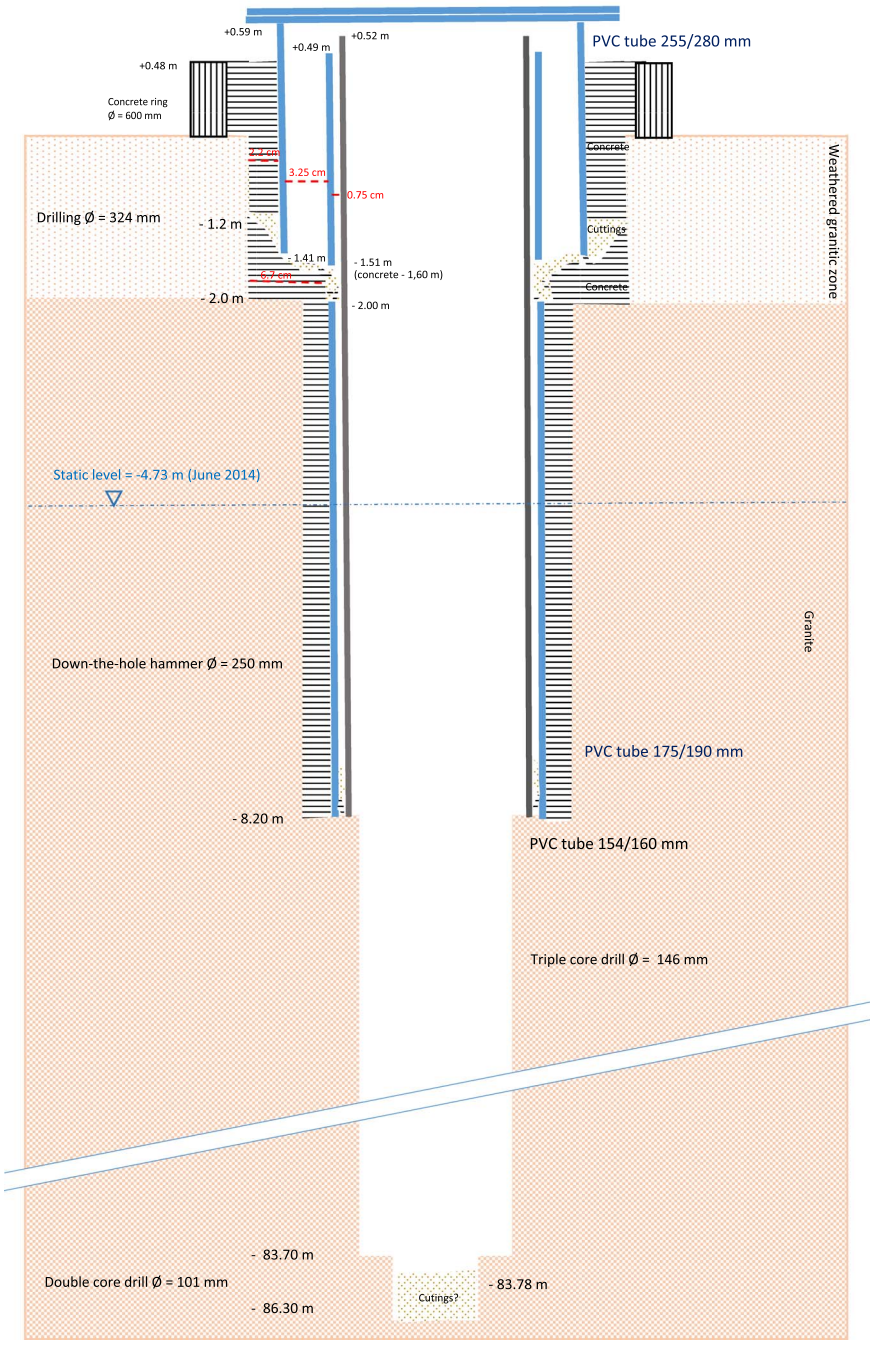

Stölben GmbH
Barlstraße 42
56856 Zell/Mosel
Tel: +49 6542 9366-0
e-mail: info@stoelben-gmbh.de

Projet N° 25058_CNRS

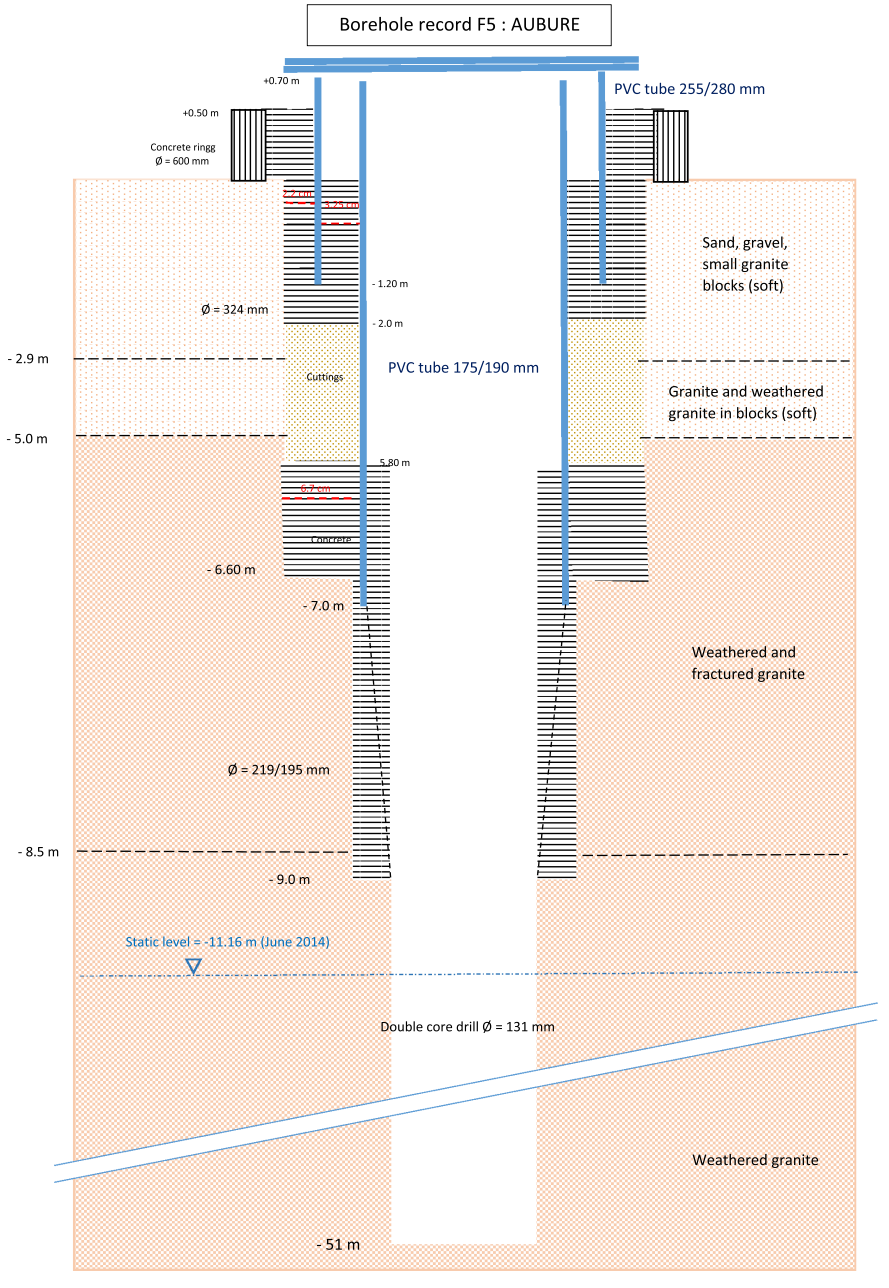

2. Presentation of the main analytical methods used for the study

2.1. *Physical–chemical logging*

After drilling the wells were emptied several times over the years 2013–2015 in order to clean them. Conductivity and temperature profiles were regularly made in the different wells with an OTT KL 010 TCM probe over the period 2015–2019. The resolution is of 0.1% of the Full Scale (FS) for the depth measurement, and the accuracy is ±0.1% of the FS for the temperature and ±0.5% of the conductivity values calculated at 25 °C.

In 2018, an Idronaut Ocean Seven 303 multiparameter CTD probe [Négrel et al., 2008, Pauwels et al., 2015] has been used in order to establish precise depth profiles of the pH, the conductivity calculated at 25 °C (µS/cm), the temperature (°C), the redox potential (expressed in reference to the potential of the Standard Hydrogen Electrode) and the dissolved oxygen concentration (% of saturation) in the water columns of the wells. The accuracy of the pressure sensor is 0.05% full scale thus giving a relative positioning at cm scale when lowering the probe. The accuracy of the sensors reported by the manufacturer is of 1 $\mu S \cdot cm^{-1}$ for the conductivity, 0.05% for the pressure, 0.005 °C for the temperature, 0.01 for the pH, 1%sat for the oxygen and 1 mV for the redox. The uncertainty in redox measurement in natural waters can be far higher, i.e., ±50 mV [in Kölling, 2000]. The time response of the conductivity, the temperature, and the pressure sensors is of 50 ms while the response of the oxygen, the redox and the pH sensors is of 3 s. As an approximate 0.08 m/s descending speed of the probe has been used, a 0.2 m to 0.3 m accuracy on the depth of the measurements can be assumed. Physical and chemical logs have been performed prior pumping in F1a, F1b, F5, F6, F7 and F8 boreholes and in Pz3 and Pz7 piezometers. In order to evaluate the influence of pumping on the physico-chemical structure of the well, logs have been repeated shortly after pumping (within 1 h) in F5, F6, F7, F8 and Pz3. Another log was performed in F5 borehole 36 h after the pumping to evaluate the duration of the transient changes induced by this operation. During the summer 2019, additional logs have been done in F5 borehole, under ambient flow conditions (2 times) and after pumping at depth (1 time). Apart from characterizing the physical–chemical parameters of the water column, these investigations are also used as an indicator for locating zones of water production in the boreholes.

2.2. *Fracture measurements*

Within the two pits Fo-1 and Fo-3, fractures at one or two meters below the soil surface have been measured along N45°E and N100°E horizontal scanlines.

In boreholes, acoustic and optical borehole images have been performed. The two main image acquisition campaigns were done by Terratec company, in winter 2012, for boreholes F6, F7 and F8, and in June 2014, for boreholes F1a, F1b and F5. For both campaigns, an optical scanner and a Borehole Televiewer, BHTV, were used (Supplementary Table S1). The depth intervals on which such images have been recovered and their quality are given in Supplementary Table S1.

The BHTV logging provides an acoustic image of the borehole surface. The method consists of aiming an ultrasonic beam at the borehole wall. The reflected beam is analyzed in terms of amplitude and transit time. The amplitude of the received wave depends on the reflectivity of the rock, the attenuation due to fluids and the borehole geometry. The transit time provides the shape of the borehole wall. The BHTV produces a complete 360° acoustic image for both measurements (amplitude and transit time). On these images, sinusoidal traces are interpreted in terms of planar discontinuities, such as faults, fractures, bedding, etc, and can be oriented with a magnetometer, which gives the orientation of the beam according to magnetic North.

The optical scanner is a rotative camera holding also a magnetic system and giving oriented real images of the borehole walls. It has to be used in a clean borehole without water. On the contrary, the acoustic wave of BHTV needs a fluid to be circulated and is used under the water table. As with the BHTV, fractures and other planar discontinuities orientations are measured on optical images.

Thus, for the analysis of the Strengbach borehole images (Optical scanner and BHTV), sinusoidal traces were picked and correctly oriented in relation to the borehole deviation in order to obtain discontinuities orientation. For this study, only natural fractures, older than the drilling and in relation to the

Supplementary Table S3. Available borehole images in the Strengbach wells

	Borehole	Type of image logs	Logger	Date	Quality	Depth interval (m)	Total depth borehole (m)	Nb of discontinuities
	F1	Optical scanner	Terratec	03/06/2014	++	7.2–50.9	51.2	130
Cored	F1b	Optical scanner	Terratec	03/06/2014	++	8.05–83.95	86.3	183
Cored	F5	Optical scanner	Terratec	03/06/2014	+	7.5–47.9	51	155
		BHTV	Terratec	03/06/2014	+	9.1–47.2		
Cored	F6	Optical scanner	Terratec	08/11/2012	−	0–69	121	191
		BHTV	Terratec	08/11/2012	−	60–121		116
	F7	Optical scanner	Terratec	06/12/2012	+	0–55	55	28
		BHTV	Terratec	06/12/2012	−	7.3–54.7		52
	F8	Optical scanner	Terratec	27/11/2012	−	1.2–36.4	51	53
		BHTV	Terratec	27/11/2012	−	1.6–47.8		

tectonic history of the rocks, are considered. Few induced fractures, such as vertical or "en échelon" fractures, formed during the drilling and in relation with the present-day stress field have been observed but not taken into account. As shear or displacement cannot be detected on images, we consider all observed fractures as mode 1 fractures.

Sinusoidal traces are not always clearly visible and their detection is not always easy depending on the image quality. In order to carry out a quality control, we have defined different quality classes of the observed sinusoidal traces: perfectly visible, more than 50% visible, less than 50% visible, etc. The orientation of the fractures has been determined independently in each of these classes. No systematic variation was observed in the orientations obtained from one class to another. Therefore, all classes were taken into account in the results.

The quality of the images is very important for a good image analysis and fracture picking. In our case, the image quality is not homogeneous and has an impact on the fracture detection. Globally, images in F1a, F1b and F5, on the south part of the watershed, have good to very good quality and the data set could be considered as reference (Supplementary Table S3). On the contrary, images in F6, F7 and F8 have bad to very bad quality (Supplementary Table S3). Some parts of the images are partly or totally dark and no fracture can be correctly detected.

On two pits, Fo-1 and Fo-3, fracture orientations have been measured along scanlines following two perpendicular direction to avoid the direction bias. The scanlines have been located 2 m under the surface in the most unaltered granite.

2.3. *Porosity and permeability determination*

Rock samples representative of the main geological types observed were collected along the F1b, F5 and F6 cores. When possible, core samples were drilled either perpendicularly or parallel to their vertical axis to get cylindrical cores with a length of 40 mm and a diameter of 20 mm for porosity and permeability determination. When the drilling of core samples was not possible, samples without precise shape were extracted from the cores for porosity determination. A total of 66 cores (29 in F1b, 14 in F5 and 23 in F6) and 12 shapeless samples were treated. Location of the samples are given in Supplementary Table S2.

Before any treatment, all samples were vacuum dried at 40 °C for 24 h and saturated with deionized water. The porosity of the samples was measured by using the triple-weighing method: the successive measurements of the dry, saturated and saturated immersed specimen masses lead to the determination of the connected porosity [Luquot et al., 2016].

Permeability to water was measured on 52 cores (15 in F1b, 14 in F5 and 23 in F6) previously saturated with deionized water. Permeability measurements were carried out in a 200 MPa hydrostatic pressure cell equipped with a pore fluid pressure circuit [Reuschlé, 2011]. The entire apparatus was thermally regulated at 30 °C to keep pressures constant in the absence of imposed pressure changes. Samples were inserted in a viton jacket clamped on end-pieces to apply a constant confining pressure of 2 MPa for all tests, a minimum value that ensured that there was no water flow between the jacket and the sample

without altering the microstructure of the sample. Permeability was measured either by the steady-state method (for high permeabilities) or the pulse decay method (for low permeabilities).

For the steady-state method, the volumetric water flow rate Q through the sample is measured for a constant pore fluid pressure difference ΔP across the sample. The permeability k to water is then calculated using Darcy's relation:

$$k = \eta \frac{LQ}{S\Delta P} \tag{1}$$

where η is the viscosity of water (= 10^{-3} Pa·s), L and S are the sample length and cross-sectional area. The pressure difference ΔP was kept constant and equal to 0.5 MPa.

For the pulse decay method [Bernabé, 1987], a positive pressure difference ΔP (= 0.5 MPa) was imposed in the upstream pore fluid section. This difference was then free to return to zero through the sample. The differential pore fluid pressure decay is approximately exponential and the decay time is inversely proportional to the permeability [Hsieh et al., 1981]:

$$\Delta P(t) \propto \exp(-\alpha t) \tag{2}$$

and

$$\alpha = \frac{Sk(C_u + C_d)}{\eta L C_u C_d} \tag{3}$$

where t is time, and C_u (=3.957×10^{-9} m^3/MPa) and C_d (=4.828×10^{-9} m^3/MPa) are the compressive storages of the upstream and downstream pore fluid sections, respectively.

3. Petrological description of cores F1b, F5 and F6 (and Supplementary Figure S1)

The main macroscopic, lithological and petrological characteristics of cores from F1b, F5 and F6 boreholes are described below. The F6 core crosscuts first gneiss injected by granite down to 42 m depth and then a porphyry granite similar to that observed on the southern slope. The three drill cores have been subdivided into four classical horizons: a soil horizon of limited vertical extension, an unconsolidated saprolite level, and an in-place fractured bedrock, subdivided in a saprock zone in the upper part and a fractured bedrock in the lower part. The saprock horizon corresponds to horizon marked by an high density of open sub-horizontal fractures and the deep bedrock horizon by the presence of almost exclusively of steep dip fractures (see Section 4.1).

In the F1b borehole, the soil horizon relies on granitic arena horizons formed of sand associated with a matrix of clay particles and iron hydroxides, containing millimetric to decimetric reddish blocks of altered bedrock which are likely not in place. At ~1.9–2.0 m depth, the mobile regolith passes over a short distance to the saprock zone marked by in-place 5 to 10 cm wide blocks of fractured and altered granite. The saprock horizon extends up to ≈3.3 m depth. Below, the rock is more massive, interspersed with fractures or cataclastic fractured zones showing evidences of water circulation and traces of water-rock interactions at its walls. In both levels, the alteration of granite is characterized by pinky to reddish plagioclase grains, whitish to pinky K-feldspar grains and dark masses of iron hydroxides replacing biotite. Fractures include a network of sub-horizontal cracks in addition of more vertical fractures. Both fractures and cracks are impregnated by iron hydroxides. The proportion of altered granite characterized by a pinky to redish colour compared to a more grey and massive granite decreases with depth in the fractured bedrock. Below ~73 m, the bedrock consists most exclusively of a grey and massive granite interspersed with sub-vertical fractures or cataclases. Subhorizontal cracks are absent. Primary feldspars and biotite are better preserved. Alteration of these minerals and iron hydroxides are limited to sub-vertical fractures.

In the F5 borehole, the soil horizon relies on granitic arena horizons which extend down to 9 m deep and contain millimetric to decimetric reddish blocks of altered bedrock. These horizons are almost exclusively formed of gravels down to 5 m, followed by a zone containing more 5–10 cm-wide rock pieces before intersecting again a true gravel zone at 8–9 m depth. The upper saprolite horizons contain pieces of altered bedrocks showing remobilization evidence. They are therefore considered as colluvium levels, whose vertical extension at depth is difficult to define. At depths of 5 m and more, the subhorizontal structures observed could mark rather in place granitic arena horizons. In F5, below 9 m depth, the granite is in place, altered and fractured. There the core is made of 5–10 cm-wide pieces down to 12–13 m depth. This zone is marked by a high degree of fracturation and alteration, which makes the

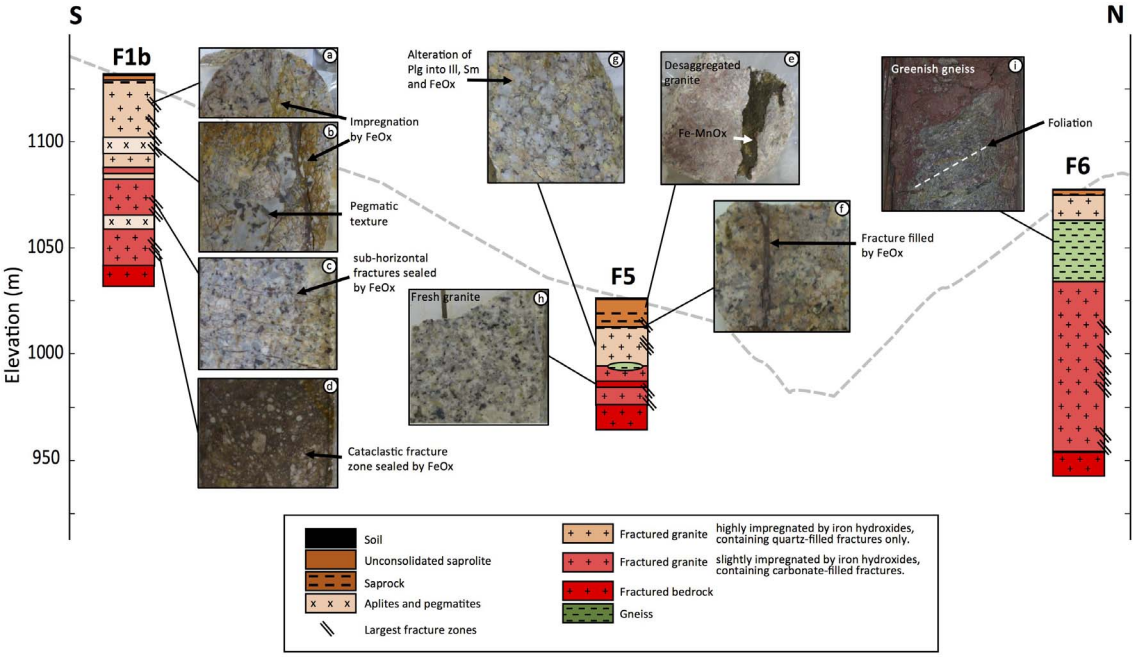

Supplementary Figure S1. Geological logs of the three cored boreholes (F1b, F5, and F6) indicating the different lithologies (granite, aplite/pegmatites, and gneiss), major fractures, and the four major horizons defined from the macroscopic observations (soil, mobile saprolite, saprock, and in-place fractured bedrock). The latter distinguishes an upper part, which is highly impregnated by iron hydroxides and contains quartz-filled fractures only, and a lower part, which is less impregnated by iron hydroxides and contains carbonate-filled fractures. The logs are at scale. Nine additional photographs illustrate the different lithologies and the horizons in the three cored boreholes. F1b borehole: (a) granite fractured and highly impregnated by iron hydroxides (F1b-12 m); (b) pegmatite fractured and highly impregnated by iron hydroxides (F1b-32 m); (c) granite in the fractured and less impregnated by iron hydroxides (F1b-54 m); (d) cataclastic fractured zone sealed by iron-hydroxides (F1b-86 m). F5 borehole: (e) partially disagreggated granite in saprolite (F5-6 m); (f) granite in the saprock (F5-13 m); (g) granite fractured and highly impregnated by iron hydroxides (F5-27 m); (h) fresh grey granite (F5-41 m). F6 borehole: (i) gneiss (F6-31 m). Abbreviations: FeOx iron hydroxides, Plg plagioclase, Sm smectite, Ill illite.

granite relatively weakened and friable with a large proportion of open subhorizontal fractures. It is defined as the saprock horizon of the core. Below 12–13 m depth, the granite is less fractured leading to massive, cohesive core sections with a thickness of 20 to 30 cm or more. Plagioclase is reddish, K-feldspar is whitish to pinky and biotite occurs as dark masses, and iron hydroxides impregnate cracks in granite down to ~32 m. Below, the granite becomes grey.

In borehole F6 like in borehole F1, the transition between mobile regolith and the in-place gneiss of the saprock horizon is around 2.5 m, and the transition between saprock and fractured gneiss horizons around 3.3 m–3.5 m. Below, down to 42 m, gneiss is highly altered, reddish and fractured, inducing locally weakness and friability of the rock associated with impregnation with iron hydroxides. At ~42 m, gneiss is in contact with granite. Granite is whitish, consolidated and affected by fracture network filled with iron hydroxides giving locally ocher to reddish color. The whitish color of the matrix is partially associated with silicification of feldspar. Below ~47–48 m down to 120 m, granite becomes greyish to pinky due

to alteration of plagioclase with slight impregnation of iron-hydroxides. Between 63 and 75 m, granite is affected by several fracture/faults and the drilled rock often consists of crushed granite. Below 75 m, granite is fractured but remains consolidated, and fractures are often sealed.

4. Conductivity loggings in borehole F1b and origin of its time variations (and Supplementary Figure S2)

Boreholes F1a and F1b were drilled near one of the summits of the southern slope of the watershed, about ten meters from each other (Figure 2 main text). As detailed in Ranchoux [2020], the high conductivity values analysed in the F1a borehole water, with values systematically higher than 150 μS/cm, have been interpreted as an artefact due to a probable pollution of the well by concrete leaching. Therefore the data have not be used for the current study.

It was observed also that during a pumping with a strong drawdown in borehole F1b (e.g. 49.80 m June 11, 2015), almost no drawdown is visible in borehole F1a (0.31 m). Such an observation certainly indicates no significant lateral hydraulic conductivity between the two boreholes. It can thus be assumed that borehole F1a pollution does not impact the conductivity profile of the borehole F1b.

For F1b well, conductivity profiles may look very different from one period to another, and from other wells (F5, F6, F7, F8). Especially in periods of high water or after periods of rain (logging of May 5, 2015) the conductivity profiles show higher values for surface water than for deep water (Supplementary Figure S2-a). It is also observed that in the recession period following the rainy period of May 2015, the conductivity logs carried out in May and June show higher conductivity zones, located deeper and deeper within the water column with time (Supplementary Figure S2-b). It is proposed that the high conductivity level recorded in the May 5, 2015 profile corresponds to a leaching of the concrete used to repair the upper part of the well damaged during its construction [Ranchoux, 2020]. More specifically, during the drilling operation, there was a perforation of the PVC pipe installed in the upper part of well F1b. A second pipe was placed and cement was introduced between the two pipes to plug the perforation. During this operation cement was lost and accumulated at the base of the two sleeves at a depth of ≈8 m. This cement is the most likely source or cause of the high conductivities measured in the upper part of the well during periods of high water or heavy rainfall. This interpretation is consistent with the observation of a significant increase in conductivity at ≈8 m depth in October 2017 during a F1B pumping operation (Supplementary Figure S2-c). Before the pumping, and at equilibrium conditions, the conductivity value was low (around 50 μS/cm) and the profile invariant, while the pumping operation displays a high conductivity anomaly at a depth of about 8 m, i.e. at the limit depth of the PVC pipes installed in F1b (see Supplementary Section 1) where cement may have accumulated. In the frame of the above interpretation, and in a context of a low lateral hydraulic conductivity, the logs made during the recession period after May 5, 2015 may thus represent a gradual vertical downward diffusion of surface pollution over time. We therefore propose not to take into account such logs in the current study. To characterize the conductivity profiles of F1b, we only took into account the logs performed in June and July 2015, during a period of no rainfall or of very low intensity, after the well was emptied on June 11, 2015 (Supplementary Figure S2-b).

On June 11, 2015 a pumping of about 6 h was carried out continuously with the pump close to the bottom of the well. The piezometric level drops strongly (around 50 m) and the conductivity profile is characterized by a low conductivity of about 45 μS/cm. In the days and weeks following the pumping operation, the conductivity profiles are relatively homogeneous with depth, with a gradual increase in conductivity over time, especially in the lower part of the well, from 45 μS/cm on June 7th to 50 μS/cm on July 30th. These observations therefore indicate low conductivities for the water supplying this well. If the increase in conductivity over time is not an artifact related to the cement leakage at the base of the protection tube, then it can be assumed that the well is supplied by several water inlets (at least two different), but with relatively low conductivities compared to the conductivities measured in the deep parts of the other wells (F5, F6, F7, and F8). This may be consistent with the observation along the F1b cores of several cataclastic fractured zones, recognized as preferential circulation zones in the Strengbach bedrock (see main text).

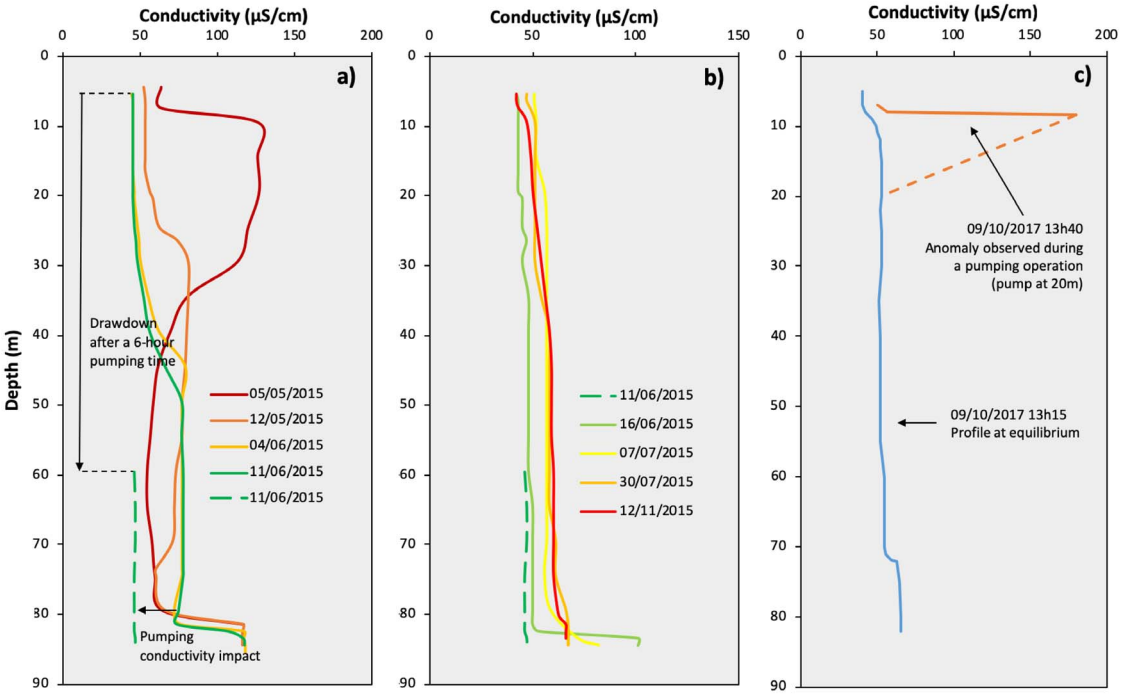

Supplementary Figure S2. Conductivity profiles in F1b borehole. For the F1b borehole, only specific periods are presented with (b) an anomaly propagation over depth and over time and (c) the natural behavior of the borehole before a new anomaly occurs in December 2015 (see text associated for more information).

References

Bernabé, Y. (1987). A wide range permeameter for use in rock physics. *Int. J. Rock Mech. Min. Sci. Geomech. Abstracts*, 24, 309–315.

Hsieh, P. A., Tracy, J. V., Neuzil, C. E., Bredehoeft, J. D., and Silliman, S. E. (1981). A transient laboratory method for determining the hydraulic properties of 'tight' rocks- I. Theory. *Int. J. Rock Mech. Min. Sci. Geomech. Abstracts*, 18, 245–252.

Kölling, M. (2000). Comparison of different methods for redox potential determination in natural waters. In Schüring, J., Schulz, H. D., Fischer, W. R., Böttcher, J., and Duijnisveld, W. H. M., editors, *Redox*. Springer, Berlin, Heidelberg.

Luquot, L., Hebert, V., and Rodriguez, O. (2016). Calculating structural and geometrical parameters by laboratory measurements and X-ray microtomography: a comparative study applied to a limestone sample before and after a dissolution experiment. *Solid Earth*, 7, 441–456.

Négrel, Ph., Roy, S., Petelet-Giraud, E., Brenot, A., Millot, R., Dutartre, Ph., and Fournier, I. (2008). Les outils de diagraphie chimique pour la caractérisation des masses d'eau : principes et exemple d'application. *Tech. Sci. Method.*, 11, 29–46.

Pauwels, H., Négrel, Ph., Dewandel, B., Perrin, J., Mascré, C., Roy, S., and Ahmed, S. (2015). Hydrochemical borehole loggings for characterizing fluoride contamination in a heterogenous aquifer (Maheshwaram, India). *J. Hydrol.*, 525, 302–312.

Ranchoux, C. (2020). *Caractérisation géochimique et datation des circulations d'eaux profondes dans la zone critique : cas du Bassin versant du Strengbach.* Phd thesis, Université de Strasbourg, France. 288 p.

Reuschlé, T. (2011). Data report: permeability measurements under confining pressure, Expeditions 315 and 316, Nankai Trough. In Kinoshita, M., Tobin, H., Ashi, J., Kimura, G., Lallemant, S., Screaton, E. J., Curewitz, D., Masago, H., Moe, K. T., and the Expedition 314/315/316 Scientists, editors, *Proceedings of the Ocean Drilling Program, 314/315/316*. Integrated Ocean Drilling Program Management International, Inc., Washington, DC.